Minichromosome maintenance helicase paralog MCM9 is dispensible for DNA replication but functions in germ-line stem cells and tumor suppression

Suzanne A. Hartford[a], Yunhai Luo[a], Teresa L. Southard[a], Irene M. Min[b], John T. Lis[b], and John C. Schimenti[a,1]

[a]Departments of Biomedical Sciences and [b]Molecular Biology and Genetics, Cornell University, Ithaca, NY 14853

Edited by R. Scott Hawley, Stowers Institute for Medical Research, Kansas City, MO, and approved September 19, 2011 (received for review August 18, 2011)

Effective DNA replication is critical to the health and reproductive success of organisms. The six MCM2–7 proteins, which form the replicative helicase, are essential for high-fidelity replication of the genome. Many eukaryotes have a divergent paralog, MCM9, that was reported to be essential for loading MCM2–7 onto replication origins in the *Xenopus* oocyte extract system. To address the in vivo role of mammalian MCM9, we created and analyzed the phenotypes of mice with various mutations in *Mcm9* and an intronic DNA replication-related gene *Asf1a*. Ablation of *Mcm9* was compatible with cell proliferation and mouse viability, showing that it is nonessential for MCM2–7 loading or DNA replication. *Mcm9* mutants underwent p53-independent embryonic germ-cell depletion in both sexes, with males also exhibiting defective spermatogonial stem-cell renewal. MCM9-deficient cells had elevated genomic instability and defective cell cycle reentry following replication stress, and mutant animals were prone to sex-specific cancers, most notably hepatocellular carcinoma in males. The phenotypes of mutant mice and cells suggest that MCM9 evolved a specialized but nonessential role in DNA replication or replication-linked quality-control mechanisms that are especially important for germ-line stem cells, and also for tumor suppression and genome maintenance in the soma.

gametogenesis | ovarian carcinoma | replication licensing | spermatogenesis | prereplication complex

The eukaryotic Mcm gene family consists of eight genes, *Mcm2* to *-7*, and in a subset of organisms, *Mcm8* and *Mcm9*. These genes encode a highly conserved, ~200-amino acid "MCM domain" containing Walker A and Walker B AAA+ ATPase motifs. MCM2 to -7 (hereafter, MCM2-7) form the DNA replicative helicase (1–3). The activities of MCM2-7 are controlled to prevent rereplication during a cell cycle (4). In both yeast and mice, each of the MCM2-7 proteins are essential, despite having structural similarity (5, 6). Dysfunction of, or decreases in MCMs can cause genome instability and cancer (6–8).

Mcm8 and *Mcm9* are both present in diverse eukaryotes, although yeast lack them and *Drosophila melanogaster* has only *Mcm8* (9, 10). *Drosophila Mcm8* is involved in meiotic recombination (9), and human *MCM8* was suggested to enable recruitment of CDC6 to replication origins (11). CDC6 is needed for loading MCM2-7 onto replication origins, and formation of the prereplication complex (pre-RC).

Mouse *Mcm9* was first described as encoding a 386 amino acid, C-terminal–truncated paralog of the MCM2-7 proteins (12). This isoform ($MCM9^S$) contains a partial MCM domain (Fig. 1) containing the Walker A-type ATPase motif, but not a Walker B domain. A larger form ($MCM9^L$) was predicted to contain both the Walker A and B motifs required for helicase activity in MCM2-7 (13). However, the canonical Walker A motif in MCMs is GDP[G/S]×[S/A]KS, but in MCM8 and -9 it is GDPG[L/T]GKS. The latter is more similar to the canonical AAA+ ATPase consensus of GxxGxGK[S/T]. The MCM9 Walker B motif is also atypical (CCIDEFNSL compared with the more canonical motif of MCM2-7 [C/V][C/L]IDEFDKM).

The first major functional study of MCM9 reported that in *Xenopus* egg extracts, MCM9 interacts with CDT1 to load MCM2-7 onto replication origins, and also counteracts the inhibitory effects of Geminin upon CDT1 for replication licensing (14). Thus, MCM9 was deemed essential for pre-RC formation and DNA replication. Here, we report that *Mcm9* is not required for pre-RC formation or DNA replication in mice, but is important for germ-line stem-cell maintenance and proliferation, genome stability, and cancer prevention.

Results

Genomic Structure of the Mouse *Mcm9* Locus and mRNA Isoforms. Although RefSeq and published *Mcm9* gene models are available (12, 13), we performed additional bioinformatic analyses and targeted RT-PCR to derive the correct structure, as shown in Fig. 1 (see also Fig. S1 and *SI Results*). *Mcm9* produces two alternative C-terminal mRNA isoforms by alternative use of a splice site within exon 7. Skipping this site results in a short isoform ($Mcm9^S$) encoding a protein of 386 aa. Splicing to exon 8 creates a longer isoform ($Mcm9^L$), encoding an 1,134-aa protein (Fig. 1*A*). $MCM9^S$ contains only half of the conserved MCM domain containing the Walker A motif (Fig. 1*B*).

The seventh intron contains another gene, *Asf1a* (Antisilencing function 1 homolog A), with a transcriptional orientation antisense to *Mcm9* (Fig. 1*A*). ASF1a is a histone chaperone with diverse functions, including the regulation of replication fork progression under normal and replication stressed conditions (15, 16). Evidence suggests it does so by interacting with MCM2-7 via a histone H3-H4 bridge to transfer histones from dissociated nucleosomes to newly forming nucleosomes in the wake of the replication fork (15).

***Mcm9* Isoforms Are Expressed Ubiquitously in Mice.** Expressed sequence tag (EST) data in Unigene show that *Mcm9* is expressed in many tissues, but does not distinguish between the two isoforms. RT-PCR analysis of $Mcm9^S$ and $Mcm9^L$ revealed expression of both in all tissues and through early development (Fig. 1*C*). Levels of transcription in the gene body were assessed by analyzing GRO-Seq (global run-on sequencing) data from ES cells and mouse embryonic fibroblasts (MEFs) (17). This method determines the amount and locations of engaged RNA polymerase on a gene at the time of the assay (18). Run-on transcripts are produced across the entire *Mcm9* gene body. The expression levels of mature transcripts indicate that the amounts of each isoform produced are similar, based on the exon sequence counts of $Mcm9^S$ and $Mcm9^L$ (19) (Fig. S2). *Asf1a* had similar amounts of engaged RNA pol II (Fig. S2).

Author contributions: S.A.H. and J.C.S. designed research; S.A.H., Y.L., T.L.S., and I.M.M. performed research; S.A.H., Y.L., T.L.S., I.M.M., and J.C.S. analyzed data; and S.A.H., J.T.L., and J.C.S. wrote the paper.

The authors declare no conflict of interest.

This article is a PNAS Direct Submission.

[1]To whom correspondence should be addressed. E-mail: jcs92@cornell.edu.

This article contains supporting information online at www.pnas.org/lookup/suppl/doi:10.1073/pnas.1113524108/-/DCSupplemental.

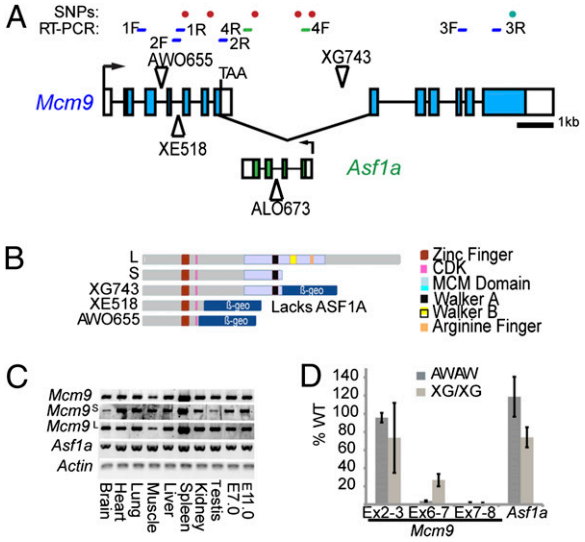

Fig. 1. *Mcm9* locus structure and isoforms. (*A*) *Mcm9* has 2 isoforms: $Mcm9^{S}$ and $Mcm9^{L}$. The former uses an alternative splice site in exon 7 that results in termination. Triangles depict the insertion sites of the gene traps. XE518 created a deletion that includes *Asf1a*. Locations of polymorphic SNPs used for measuring deletion size in the $Mcm9^{XE518}$ allele are indicated. These are: (*Left* to *Right*) rs51772485, rs46087546, rs51382030, rs51176035, rs47659858, and rs49316622. The *Asf1a* gene trap is located 640-bp downstream of exon 2. (*B*) MCM9 isoforms and the gene-trap alleles. MCM9 contains a zinc finger, CDK site, and the MCM domain. (*C*) Tissue expression of *Mcm9* and *Asf1a* by semi-qRT-PCR. Primer pairs used in the top four panels are sets 1 to 4, respectively, as shown in *A*. (*D*) qRT-PCR analysis of *Mcm9* and *Asf1a* in mutant MEFs ($n = 3$). AWO, $Mcm9^{AWO655}$; XG, $Mcm9^{XG743}$. Error bars indicate SD.

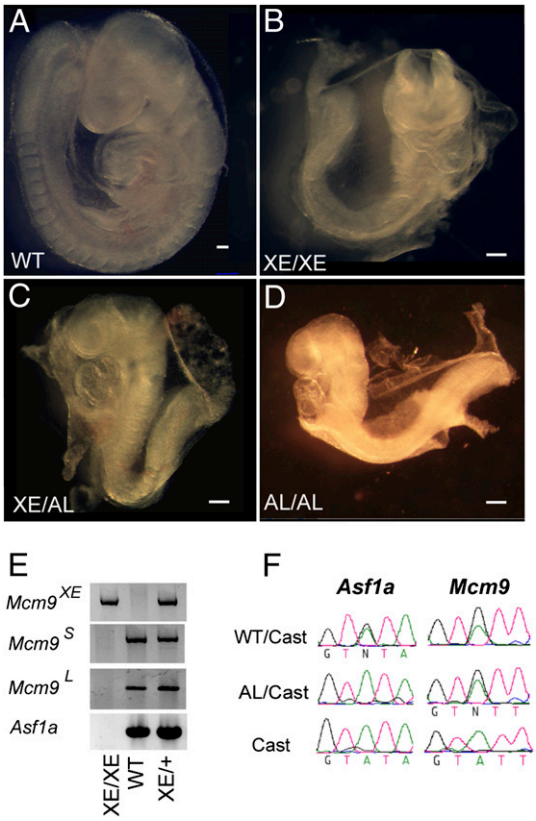

Fig. 2. Midgestation lethality in MCM9- and ASF1A-deficient embryos. (*A–D*) E9.5 embryos. (Scale bars, 500 μM.) (*E*) RT-PCR of E9.5 embryos. Primers for $Mcm9^{S}$ and $Mcm9^{L}$ are sets 2 and 3, respectively, from Fig. 1*A*. Primers (XE518WTF and XE518GTR) for $Mcm9^{XE}$ are specific for the gene-trap fusion transcript. (*F*) RT-PCR/sequencing of polymorphic coding SNPs (rs51382030 for *Asf1a*; rs51772485 for *Mcm9*). The WT allele here is C3H, which is identical to the parental 129-based gene trap chromosome. XE, $Mcm9^{XE518}$; AL, $Asf1a^{ALO673}$.

MCM9 Is Not Required for DNA Replication. To determine the in vivo function of the MCM9 isoforms, we generated mice containing three different gene-trap insertions within *Mcm9* (Fig. 1 *A* and *B*). We also generated a mutant allele of *Asf1a* ($Asf1a^{ALO673}$) to explore potential regulatory or functional relationships between the two genes.

The $Mcm9^{XE518}$ insertion actually caused a deletion beginning downstream of *Mcm9* exon 4, extending through the entire *Asf1a* gene, and terminating upstream of the final *Mcm9* exon (Fig. 1*A*). Thus, $Mcm9^{XE518}$ is null for *Asf1a* and presumably *Mcm9*. Intercrosses of $Mcm9^{XE518/+}$ mice failed to produce newborn homozygotes ($P << 0.001$ by χ^2) Table S1), indicating the allele is embryonically lethal. Timed matings revealed that $Mcm9^{XE518/XE518}$ embryos were viable at embryonic day (E) 9.5 but were smaller and developmentally arrested at a stage resembling E8.5 embryos (Fig. 2*B*). These embryos contained no detectable *Asf1a* mRNA or *Mcm9* transcripts downstream of the gene-trap insertion site (Fig. 2*E*).

Because *Asf1a* is also disrupted in the $Mcm9^{XE518}$ allele, the lethal phenotype could be a result of mutation of either gene or a combination of both. To distinguish between these possibilities, we created mice bearing the $Asf1a^{ALO673}$ gene-trap allele, which is predicted to truncate 129 C-terminal amino acids from the 209-aa protein. Homozygotes died at midgestation, with a phenotype similar to $Mcm9^{XE518/XE518}$ embryos (Fig. 2*D*). The phenotype is likely caused by loss of *Asf1a* alone because normal *Mcm9* transcripts are produced *in cis* from the $Asf1a^{ALO673}$ allele (Fig. 2*F*). As expected, $Mcm9^{XE518}$ failed to complement the lethality of $Asf1a^{ALO673}$ (Fig. 2*C* and Table S1). These data demonstrate that neither gene is required for cell division (and presumably DNA replication) during the first half of mouse gestation, a period of dramatic cell proliferation. However, these data do not reveal the developmental role of MCM9, as the lethal phenotype of *Asf1a* in the $Mcm9^{XE518}$ allele obscures or precludes potential contemporaneous or subsequent roles.

Because ASF1 physically associates with MCM2-7 and facilitates nucleosome reassembly during DNA replication and DNA repair (15, 20), processes that may overlap with MCM9, the question arises as to whether the physical arrangement of these two genes (which is conserved in mammals and chickens but apparently not zebrafish, based on current genome assemblies) is entirely coincidental. It is possible that there is a regulatory relationship between the genes, either with respect to their sharing common enhancer elements or modulators of chromatin structure, or in still more complex ways involving the complementarity of their transcripts or the interplay of the mechanics of divergent transcription complexes. However, transcription of *Mcm9* through the *Asf1a* gene is not required for *Asf1a* transcription *in cis* (Fig. 1*D*), and intact *Asf1a* is not needed for *Mcm9* transcription (Fig. 2*F*). These results indicate that if there is indeed a regulatory relationship between the genes, it is likely to be related to sharing control sequences, identical regional chromosomal structure, or posttranscriptional processing.

Mice with Severe Depletion or Elimination of *Mcm9* Are Viable. To identify the in vivo roles of each *Mcm9* isoform, two other gene-trap alleles were used that do not ablate *Asf1a*. $Mcm9^{XG743}$ is located downstream of exon 7 and *Asf1a* mRNA levels are ~75% of WT (Fig. 1*D*). $Mcm9^{XG743}$ is predicted to allow production of the entire $MCM9^{S}$ polypeptide, either as a fusion to β-geo or as the endogenous protein (Fig. 1*B*). A slight amount (<3%) of mRNA was detected that corresponds to splicing over the gene trap (exon 7–8 products). $Mcm9^{S}$ and fusion transcripts were also reduced from

DEVELOPMENTAL BIOLOGY

WT levels (Fig. 1*D*). These results indicate that *Mcm9*^{XG743} is severely hypomorphic or null for *Mcm9*^{L}, and potentially hypomorphic for *Mcm9*^{S}. Heterozygote intercrosses produced *Mcm9*$^{XG743/XG743}$ offspring at the expected Mendelian ratio (P = 0.98) (Table S1). The *Mcm9*^{AW0655} allele, which effectively terminates transcripts upstream of the entire MCM domain (Fig. 1 *A*, *B*, and *D*), thus appears null for *Mcm9* but leaves *Asf1a* transcription intact (Fig. 1*D*). *Mcm9*$^{AWO655/AWO655}$ and *Mcm9*$^{AWO655/XE518}$ animals are completely viable (Table S1). Therefore, MCM9 is unnecessary for DNA replication.

MCM9 Deficiency Causes Germ-Cell Loss. Despite being grossly normal, *Mcm9*^{XG743} male homozygotes had markedly smaller testes than WT littermates, a differential that was evident at puberty and widened over time (Fig. 3*A*). Despite a consequent 67% decrease in epididymal sperm concentration at 12 wk of age, these mutant males were fertile. Testis histology revealed three notable seminiferous tubule abnormalities (Fig. 3 *B*–*D*). The most striking abnormality was progressive germ-cell depletion. The second was the presence of seminiferous tubule sections (~5%) lacking spermatogonia (the adult germ-line stem cells), but containing differentiated meiotic spermatocytes or postmeiotic spermatids (Fig. 3*D*, arrows). The third class of abnormal tubule cross sections (5%) contained a cohort of spermatocytes arrested in meiosis (Fig. 3*D*, *Inset*). These abnormalities were also observed in *Mcm9*^{AWO655} male homozygotes and compound heterozygotes (Fig. S3). Notably, mice with severe depletion of MCM2-7 are fertile and do not exhibit these germ-cell loss phenotypes (Fig. S3) (6, 8), suggesting that the germ-cell effects in *Mcm9* mutants likely occur by mechanisms distinct from MCM2-7 helicase defects.

Young *Mcm9*$^{XG743/XG743}$ females were fertile but also exhibited germ-cell loss. Mutant 6- to 12-wk ovaries had fewer total follicles and were nearly devoid of primordial follicles. Oocytes were almost completely absent at 24 wk (Fig. 3 *E* and *F*). Most *Mcm9*$^{AWO655/AWO655}$ females were infertile and exhibited ovarian hyperplasias and tubulostromal adenomas consistent with premature ovarian failure (see below).

The sex-independent shortfall of germ cells in peripubertal animals is suggestive of a defect early in the germ lineage, possibly during the expansion or establishment of germ-line stem-cell pools during embryonic development. To test this, control and *Mcm9*$^{XG743/XG743}$ gonads were serially sectioned and probed with the germ-cell–specific marker MVH (mouse vasa homolog). This process revealed a 72% decrease of gonocytes in nascent seminiferous tubules (Fig. 3 *G*–*I*), and 82% fewer oocytes in newborn ovaries (Fig. 3 *J*–*L*). Therefore, the shortfall in germ cells occurred during gestation. To determine if germ-cell loss occurs via TRP53-pathway–mediated elimination, *Mcm9*$^{XG743/XG743}$ *Trp53*$^{-/-}$ and *Mcm9*$^{XG743/XG743}$ *Cdkn1a*$^{-/-}$ (*Cdk1na* = *p21*) animals were bred and their germ-cell numbers were scored at 1 d postpartum (dpp). There was no rescue of germ-cell depletion in either of these compound mutants (Fig. 3 *I* and *L*). Curiously, TRP53 deficiency actually further decreased the numbers of germ cells in *Mcm9*$^{XG743/XG743}$ newborn males but not females (Fig. 3 *I* and *L*).

MCM9 Deficiency Does Not Impact MCM2-7 Chromatin Loading, Has Minimal Impact on Genome Stability, but Predisposes to Cancer. Mutations reducing MCM2-7 levels cause genomic instability and cancer susceptibility in mice (7, 8) as a consequence of decreased pre-RC formation (6, 21, 22). Because it was reported that MCM9 is essential for MCM2-7 loading onto replication origins and thus pre-RC formation in *Xenopus* oocyte extracts (14), we tested whether MCM9 depletion impacts MCM2-7 chromatin loading in *Mcm9* $^{AWO655/AWO655}$ MEFs. No difference in chromatin-bound MCM2, MCM4, and MCM7 was observed (Fig. 4 *A* and *B*). Furthermore, in contrast to *Xenopus* oocyte extracts immunodepleted for MCM9, no decrease of CDT1 was observed in mutant MEFs (Fig. 4 *A* and *B*).

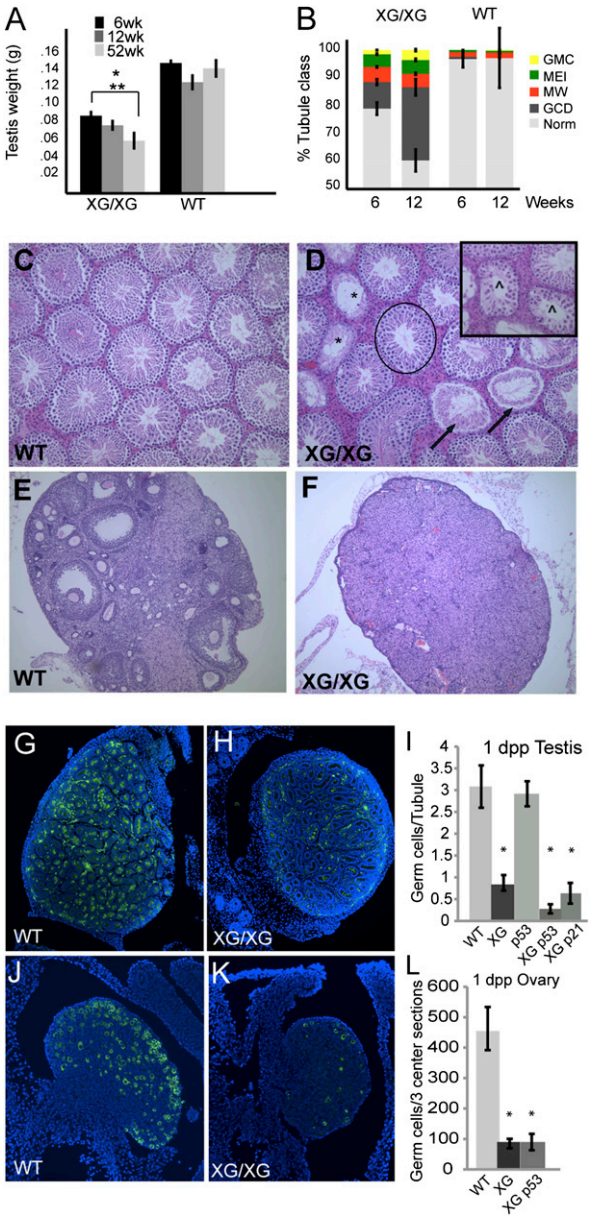

Fig. 3. *Mcm9* mutations cause germ-cell depletion and loss of spermatogonial stem cells. (*A* and *B*) Quantification of testis weights and histological abnormalities. *Significantly different from WT; **significant decrease in mutant testis size over time (n = 10). Abbreviations in *B* for seminiferous tubule cross sections that contain or exihibit the following: GMC, giant multinucleated cells; MEI, meiotic arrest; MW, missing wave of spermatogenesis; GCD, germ-cell depletion; Norm, normal. (*C* and *D*) H&E-stained histological sections of testes from 12-wk-old mice of the indicated genotypes. WT, wild-type; XG, *Mcm9*^{XG743} (magnification: 200×). Error bars indicate SD. Seminiferous tubules marked with an asterisk (*) are devoid of germ cells; those marked with a caret (^) exhibit meiotic arrest (*Inset*); and those indicated by arrows are depleted of spermatogonia but undergoing a final wave of spermatogenesis. Circled tubules are examples of normal spermatogenesis. (*E* and *F*) H&E-stained histological sections of ovaries from 24-wk-old mice of the indicated genotypes. (*G*–*L*) Immunofluorescence of 1-dpp testes (*G* and *H*) and ovaries (*J* and *K*) of the indicated genotypes (magnification: 200×). MVH (green) stains germ cells and DAPI stains nuclei (blue). (*I* and *L*) Germ-cell counts from MVH staining data at 1 dpp (n = 3). *Significant difference vs. WT (see *Materials and Methods*). XG, *Mcm9*$^{XG743/XG743}$; p53, *Trp53*$^{-/-}$; p21, *Cdkn1a*$^{-/-}$. Error bars indicate SD.

To test for somatic chromosome instability, we measured peripheral blood micronucleus levels, an indicator of chromosome instability that is elevated in *Mcm2-7*–deficient mice (6, 8).

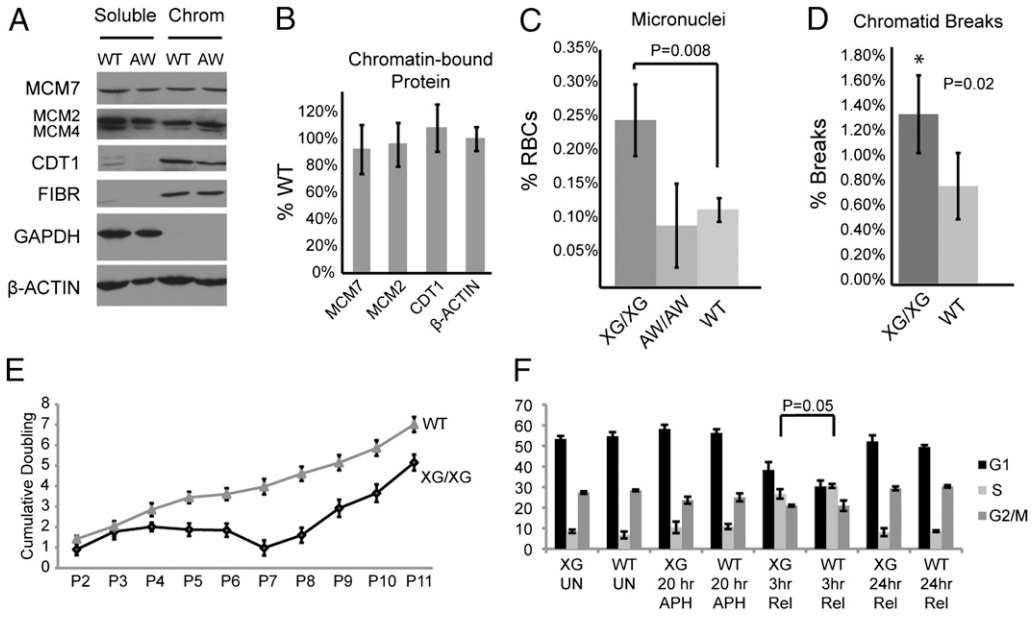

Fig. 4. Loss of MCM9 does not alter MCM2-7 or CDT1 levels, however, leads to mild genomic instability and cell-cycle defects under replication stress. (*A*) Western blots of mutant and WT MEFS showing detergent soluble vs. chromatin bound levels of indicated proteins. (*B*) Quantification of data in *A*. (*C*) Micronucleus levels in erythrocytes. (*D*) Chromatid breaks in mutant MEFS. (*E*) *Mcm9* mutant MEFs undergo premature senescence. The *y*-axis values were taken every 3 d upon passage. (*F*) Mutant MEFs exhibit a delay in cell-cycle entry following APH-induced replication stress. Primary data are in Fig. S3. MEFs were serum-starved to synchronize at G0/G1, serum was then added, then measurements were taken. AW, $Mcm9^{AWO655}$; XG. $Mcm9^{XG743}$. The *P* value is based on *t* testing. UN, measurements 20 h after serum addition, but untreated with APH; 20 hr APH, same as previous, but with APH treatement; 3hr Rel or 24hr Rel, same as previous, but 3 h or 24 h after APH was removed from media ($n = 3$). Error bars indicate SD.

Relative to WT, micronucleus levels were marginally higher in $Mcm9^{XG743/XG743}$ but not $Mcm9^{AWO655/AWO655}$ mice (Fig. 4*C*). We also observed a 1.6-fold increase in metaphase chromatid breaks in $Mcm9^{XG743/XG743}$ MEFs (Fig. 4*D*).

Although *Mcm9* disruption had no apparent impact on MCM2-7 homeostasis in MEFs and only slightly increased chromosomal instability, we aged *Mcm9* homozygotes, compound heterozygotes, and control siblings to assess potential long-term health consequences. All mutant males developed tumors by 1 y of age (vs. 32–33% of heterozygote and WT controls) (Table 1). The most remarkable difference compared with controls was in the incidence of hepatocellular carcinoma (HCC; 8 of 13 mutants vs. 0 of 28 controls). Furthermore, eight of eight affected animals had multiple HCCs (Table S2). MCM9-deficient females were prone to ovarian tumors (10 of 22 vs. 0 of 12 in controls) by 1 y of age (Table 1).

MCM9 Deficiency Does Not Perturb the Cell Cycle, but Does Delay Cell Cycle Reentry Following Replication Stress. To determine if *Mcm9* deficiency alters the cell cycle as does depletion of MCM2-7 (8, 23), $Mcm9^{XG743/XG743}$ primary MEFs (made from C3H congenic embryos) were evaluated under normal or replication stressed conditions. Continuous cultures of early passage cells were no different from WT with respect to proliferation, BrdU incorporation, and cell-cycle profile (Fig. S4 *A*–*E*). However, the mutant cultures underwent senescence prematurely (by passage 5), ultimately producing immortalized survivors (Fig. 4*E*). When $Mcm9^{XG743/XG743}$ and WT MEFs were synchronized at G0/G1 by serum starvation, then released (by serum addition) in the presence of aphidicolin (APH), APH-treated (but not untreated) mutant cells exhibited a delay in progression from G0/G1 through S-phase (Fig. 4*F* and Fig. S4*G*). These results confirm that MCM9 is dispensable for unperturbed DNA replication in mouse cells,

Table 1. Tumor incidence in MCM9-deficient mice

Genotype	Age (wk)	#	*N*	HCC (males)/OvT (females)	HA (males)/OvH (females)	Oth	Tumor-free
Males							
WT	40–55	9	≥*N*5	0	2	1	67%
$Mcm9^{GT/+}$	40–55	19	≥*N*4	0	6	1	68%
$Mcm9^{GT/GT}$	40–55	13	≥*N*4	8	4	1	0%
Females							
Controls	31–66	12	≥*N*2	0	1	1	92%
$Mcm9^{GT/GT}$	32–56	7	≥*N*2	4	2*	1	29%
$Mcm9^{GT/GT}$	9–25	15	<*N*3	6	3	2	47%

N = number of backcross generations into strain C3H; HCC, hepatocellular carcinoma; HA, hepatocellular adenoma; Oth, other tumors; OvT, ovarian tumor; OvH, ovarian hyperplasia; WT, wild-type; GT, $Mcm9^{XE518}$, $Mcm9^{XG743}$, or $Mcm9^{AWO655}$; #, number of mice. *OvH in contralateral ovary to tumor. In females, "Controls" include both heterozygotes and WT animals. Data on all individuals are presented in Table S2.

but its absence accelerates senescence and confers susceptibility to DNA replication stress.

Discussion

Mcm9 encodes at least two isoforms; however, the collection of mutant alleles reported here shows that neither is necessary for pre-RC formation or DNA replication in mice or mouse cells. This result was surprising, given a report that MCM9 is essential for loading MCM2-7 and thus formation of pre-RCs and DNA replication in a *Xenopus* egg extract system (14). In this widely-used model, sperm DNA added to the extract gets converted into chromatin, and a single round of replication ensues in a putatively physiological manner. That study (14) found that MCM9 binds to chromatin in an origin recognition complex-dependent manner, and by virtue of interacting directly with the essential helicase loading factor CDT1, enables MCM2-7 assembly into pre-RCs. Evaluation of MCM9's role was determined by immunodepletion, and supplementation of immunodepleted extracts with in vitro-produced *Mcm9* mRNA partially rescued MCM2-7 loading and the block in DNA replication.

We can offer theories on these contradictory data. First, amphibians and mammals may differ in the need for MCM9 in DNA replication, such that whereas it is essential in *Xenopus*, it has acquired a more specialized (e.g., germ-line stem cells) but nonessential role in mammals. In this regard, it should not be overlooked that the *Xenopus* oocyte is a specialized cell. Many eukaryotes lack *Mcm9* (and *Mcm8*), which supports the idea that MCM9 evolved to have a specialized role, rather than an essential one for DNA replication in some species. Second, the *Xenopus* egg extract system may not be entirely accurate in recapitulating all aspects of DNA replication and its regulation. Third, it is possible that, despite rigorous controls (14), the MCM9 immunodepletion had an unknown, deleterious effect upon pre-RC formation. Furthermore, because CDT1 interacts directly with MCM2-7 in vivo (24), MCM9 would not be required to mediate the essential CDT1:MCM2-7 interaction needed for loading. Whatever the reason for the disparity in results, the present study underscores the importance of in vivo genetic ablation studies to reveal the true physiological role of genes in the context of a whole animal.

Although *Mcm9* is ubiquitously expressed, its ablation appears to affect only a subset of tissues in the mouse under normal laboratory conditions. There were two major phenotypes: germ-cell depletion and cancer susceptibility. The observed germ-cell loss appears to occur at two stages. First, the shortfall observed at birth must have its roots in: (*i*) the specification or proliferation of the primordial germ cell (PGC) lineage; (*ii*) migration of the PGCs to the genital ridges and primitive gonads; or (*iii*) proliferation within the primitive gonads. This germ-cell proliferation happens rapidly, expanding the number from ~100 to >20,000 (25). Alternatively, PGCs may get depleted because of a failure in maintenance after migration to the primitive gonads. The second stage of loss is specific to males, where there appears to be a defect in spermatogonial self-renewal during adulthood. How MCM9 deficiency causes these defects is not clear. Although MCM9 is related to the MCM2-7 replicative helicase proteins, we do not believe that overall DNA replication per se is impaired, because severely hypomorphic MCM2-7 mutations do not have germ-cell defects. Rather, we conjecture that given the observed phenotypes of cancer susceptibility, genomic instability, and replication stress sensitivity, that MCM9 deficiency causes a subtle defect in repair of replication-induced damage to which rapidly proliferating germ-line stem cells are especially sensitive. If true, this defect might trigger cell death as a means to prevent transmission of a compromised genome to offspring. However, like DNA damage- or replication stress-induced apoptosis of ES cells (26), such death would have to occur via a TRP53-independent pathway, as indicated by our genetic studies. Alternatively, the progressive loss of spermatogonial stem cells in adult male *Mcm9* mutants points to stem-cell maintenance or proliferation defects. Future experiments will be geared toward identifying the stages at which germ cells are being lost during development, and what cell cycle and damage checkpoint pathways might be activated to cause their elimination or failure to proliferate.

Interestingly, *Mcm9* mutant mice were susceptible to distinct sex-specific cancers. Males were highly prone to HCC. In humans, HCC is more common in males than females (27). The majority of HCC mouse models are driven by viral induction, drug treatments, deregulated oncogenes, or a combination of these (28, 29). We are aware of only one germ-line mutation (*Abcb4/Mdr2*) that causes a high incidence of HCC formation with <1 y latency (30). Therefore, the *Mcm9* mutants may provide a useful model for genetic susceptibility to HCC. Mutant females were prone to ovarian tumors, although these may be related to germ-cell depletion and premature ovarian failure (31). In conclusion, MCM9 depletion drives neoplasia by a mechanism that does not seem to involve a major increase in chromosome instability or disrupted loading of MCM2-7 onto pre-RCs. However, the delayed ability of mutant MEFs to re-enter the cell cycle following APH treatment suggests that certain cell types may have a sensitivity to replication stress, and this may play a role in the cancer susceptibilities.

Materials and Methods

Mice. Gene-trap–bearing ES cell lines (from 129 substrains) were obtained from BayGenomics (XG743 and XE518) and The Sanger Institute (AWO655 and ALO673). Chimeras were generated by microinjection of the ES cells into C57BL/6J blastocysts using standard procedures. Following germ-line transmission, alleles were backcrossed into C3HeB/FeJ^{a} ("C3H"). Exact insertion sites of gene-trap vectors were determined by "primer walking," as previously described (6, 8). Genotyping was performed either by PCR amplification of the *neo* gene within the vector, by insertion-specific assay, or using polymorphic flanking microsatellite markers *D10Mit20* and *D10Mit194* that are polymorphic between 129 and C3H (Table S3). The use of mice in this study was approved by Cornell's Institutional Animal Care and Use Committee, Protocol #2004-0038 to J.C.S.

Histology and Immunohistochemistry. For basic histology, tissues were fixed in 4% paraformaldehyde overnight, paraffin-embedded, sectioned, and stained with H&E. For germ-cell counts, 10-μM sections of 1-d-old gonads were immunostained as previously described (32). Antibodies: Rabbit anti-DDX4/MVH (Abcam ab13840; 1:250); goat anti-rabbit Alexa 488 conjugate (Molecular Probes A11008; 1:1,000). Germ cells were counted in three sections from the midportion of each gonad and averaged. The data were analyzed using one-way ANOVA with Bonferroni correction (Prism software package). The resulting P values were used to determine significance ($P < 0.05$).

RT-PCR and cDNA Analysis. Semiquantitative PCR analysis of various mouse tissues (Fig. 1*C*) was performed on the Mouse Multiple Tissue cDNA panel from Clontech (636745). Real-time RT-PCR was performed as previously described (6, 8). Oligonucleotide primers are listed in Table S3.

MEF Growth Studies. MEF growth analyses and metaphase spreads were performed as previously described (33). For senescence assays, cells were counted every 3 d and replated at 5×10^5. All MEFs were derived from C3HeB/FeJ congenic (N10) embryos and were primary cultures.

Micronucleus Assays. Micronucleus assays were performed essentially as previously described (34).

Isolation of Protein Fractions. For Western analyses of chromatin bound vs. nonchromatin-bound proteins, we used a Triton-100 detergent fractionation protocol. Briefly, MEFs were trypsinized, washed twice in cold PBS, resuspended by vortexing in 1 mL TX-NE (320 mM sucrose, 7.5 mM $MgCl_2$, 10 mM Hepes, 1% Triton X-100, plus protease inhibitor), and incubated on ice for 30 min. Nuclei were pelleted (500 × *g*, 3 min) and the supernatant, containing proteins of cell membrane, cytosolic, and free forms of MCMs, was designated as the detergent "soluble" fraction (23, 35). The nuclear pellet was resuspended in 0.5 mL RIPA, liberating the chromatin fraction containing nuclear scaffold pro-

teins, DNA, and chromatin binding forms of MCMs. Antibodies used were as follows. MCM2: ab31159 (Abcam); MCM7: ab2360 (Abcam); β-actin: A1978 (Sigma); Fibrillarin: ab5821 (Abcam), CDT1: 06–1295 (Millipore), GAPDH: 6C5 (Advanced Immunochemical).

ACKNOWLEDGMENTS. We thank R. Munroe for embryonic stem cell microinjections, and C. Chuang and M. Wallace for providing tissue samples. This work was supported by grants from the New York Stem Cell Foundation (to J.C.S.), and National Institutes of Health Grant T32 HD052471 (training slot to S.A.H.).

1. Bochman ML, Schwacha A (2008) The Mcm2-7 complex has in vitro helicase activity. *Mol Cell* 31:287–293.
2. Labib K, Tercero JA, Diffley JF (2000) Uninterrupted MCM2-7 function required for DNA replication fork progression. *Science* 288:1643–1647.
3. Moyer SE, Lewis PW, Botchan MR (2006) Isolation of the Cdc45/Mcm2-7/GINS (CMG) complex, a candidate for the eukaryotic DNA replication fork helicase. *Proc Natl Acad Sci USA* 103:10236–10241.
4. Blow JJ, Dutta A (2005) Preventing re-replication of chromosomal DNA. *Nat Rev Mol Cell Biol* 6:476–486.
5. Tye BK (1999) MCM proteins in DNA replication. *Annu Rev Biochem* 68:649–686.
6. Chuang CH, Wallace MD, Abratte C, Southard T, Schimenti JC (2010) Incremental genetic perturbations to MCM2-7 expression and subcellular distribution reveal exquisite sensitivity of mice to DNA replication stress. *PLoS Genet* 6:e1001110.
7. Pruitt SC, Bailey KJ, Freeland A (2007) Reduced Mcm2 expression results in severe stem/progenitor cell deficiency and cancer. *Stem Cells* 25:3121–3132.
8. Shima N, et al. (2007) A viable allele of Mcm4 causes chromosome instability and mammary adenocarcinomas in mice. *Nat Genet* 39:93–98.
9. Blanton HL, et al. (2005) REC, *Drosophila* MCM8, drives formation of meiotic crossovers. *PLoS Genet* 1:e40.
10. Liu Y, Richards TA, Aves SJ (2009) Ancient diversification of eukaryotic MCM DNA replication proteins. *BMC Evol Biol* 9:60.
11. Volkening M, Hoffmann I (2005) Involvement of human MCM8 in prereplication complex assembly by recruiting hcdc6 to chromatin. *Mol Cell Biol* 25:1560–1568.
12. Yoshida K (2005) Identification of a novel cell-cycle-induced MCM family protein MCM9. *Biochem Biophys Res Commun* 331:669–674.
13. Lutzmann M, Maiorano D, Méchali M (2005) Identification of full genes and proteins of MCM9, a novel, vertebrate-specific member of the MCM2-8 protein family. *Gene* 362:51–56.
14. Lutzmann M, Méchali M (2008) MCM9 binds Cdt1 and is required for the assembly of prereplication complexes. *Mol Cell* 31:190–200.
15. Groth A, et al. (2007) Regulation of replication fork progression through histone supply and demand. *Science* 318:1928–1931.
16. Groth A, et al. (2005) Human Asf1 regulates the flow of S phase histones during replicational stress. *Mol Cell* 17:301–311.
17. Min IM, et al. (2011) Regulating RNA polymerase pausing and transcription elongation in embryonic stem cells. *Genes Dev* 25:742–754.
18. Core LJ, Waterfall JJ, Lis JT (2008) Nascent RNA sequencing reveals widespread pausing and divergent initiation at human promoters. *Science* 322:1845–1848.
19. Cloonan N, et al. (2008) Stem cell transcriptome profiling via massive-scale mRNA sequencing. *Nat Methods* 5:613–619.
20. Mousson F, Ochsenbein F, Mann C (2007) The histone chaperone Asf1 at the crossroads of chromatin and DNA checkpoint pathways. *Chromosoma* 116:79–93.
21. Kunnev D, et al. (2010) DNA damage response and tumorigenesis in Mcm2-deficient mice. *Oncogene* 29:3630–3638.
22. Kawabata T, et al. (2011) Stalled fork rescue via dormant replication origins in unchallenged S phase promotes proper chromosome segregation and tumor suppression. *Mol Cell* 41:543–553.
23. Ibarra A, Schwob E, Méndez J (2008) Excess MCM proteins protect human cells from replicative stress by licensing backup origins of replication. *Proc Natl Acad Sci USA* 105:8956–8961.
24. Zhang J, et al. (2010) The interacting domains of hCdt1 and hMcm6 involved in the chromatin loading of the MCM complex in human cells. *Cell Cycle* 9:4848–4857.
25. McLaren A (2003) Primordial germ cells in the mouse. *Dev Biol* 262:1–15.
26. Aladjem MI, et al. (1998) ES cells do not activate p53-dependent stress responses and undergo p53-independent apoptosis in response to DNA damage. *Curr Biol* 8: 145–155.
27. El-Serag HB (2004) Hepatocellular carcinoma: Recent trends in the United States. *Gastroenterology* 127(5, Suppl 1):S27–S34.
28. Heindryckx F, Colle I, Van Vlierberghe H (2009) Experimental mouse models for hepatocellular carcinoma research. *Int J Exp Pathol* 90:367–386.
29. Fausto N, Campbell JS (2010) Mouse models of hepatocellular carcinoma. *Semin Liver Dis* 30:87–98.
30. Mauad TH, et al. (1994) Mice with homozygous disruption of the mdr2 P-glycoprotein gene. A novel animal model for studies of nonsuppurative inflammatory cholangitis and hepatocarcinogenesis. *Am J Pathol* 145:1237–1245.
31. Vanderhyden BC, Shaw TJ, Ethier JF (2003) Animal models of ovarian cancer. *Reprod Biol Endocrinol* 1:67.
32. Reinholdt LG, Munroe RJ, Kamdar S, Schimenti JC (2006) The mouse *gcd2* mutation causes primordial germ cell depletion. *Mech Dev* 123:559–569.
33. Shima N, Munroe RJ, Schimenti JC (2004) The mouse genomic instability mutation chaos1 is an allele of Polq that exhibits genetic interaction with Atm. *Mol Cell Biol* 24: 10381–10389.
34. Reinholdt L, Ashley T, Schimenti J, Shima N (2004) Forward genetic screens for meiotic and mitotic recombination-defective mutants in mice. *Methods Mol Biol* 262:87–107.
35. Frisa PS, Jacobberger JW (2010) Cytometry of chromatin bound Mcm6 and PCNA identifies two states in G1 that are separated functionally by the G1 restriction point. *BMC Cell Biol* 11:26.